Research Article

INTERNATIONAL JOURNAL OF ADVANCED ROBOTIC SYSTEMS

International Journal of Advanced Robotic Systems
March-April 2017: 1–15

DOI: 10.1177/1729881417694290
journals.sagepub.com/home/arx
SAGE

Fractional-order sliding mode control for a class of uncertain nonlinear systems based on LQR

Dong Zhang[1], Lin Cao[2] and Shuo Tang[1]

Abstract

This article presents a new fractional-order sliding mode control (FOSMC) strategy based on a linear-quadratic regulator (LQR) for a class of uncertain nonlinear systems. First, input/output feedback linearization is used to linearize the nonlinear system and decouple tracking error dynamics. Second, LQR is designed to ensure that the tracking error dynamics converges to the equilibrium point as soon as possible. Based on LQR, a novel fractional-order sliding surface is introduced. Subsequently, the FOSMC is designed to reject system uncertainties and reduce the magnitude of control chattering. Then, the global stability of the closed-loop control system is analytically proved using Lyapunov stability theory. Finally, a typical single-input single-output system and a typical multi-input multi-output system are simulated to illustrate the effectiveness and advantages of the proposed control strategy. The results of the simulation indicate that the proposed control strategy exhibits excellent performance and robustness with system uncertainties. Compared to conventional integer-order sliding mode control, the high-frequency chattering of the control input is drastically depressed.

Keywords

Fractional control, sliding mode control, linear-quadratic regulator, uncertain nonlinear system.

Date received: 5 September 2016; accepted: 3 January 2017

Topic: Special Issue - Intelligent Flight Control for Unmanned Aerial Vehicles
Topic Editor: Mou Chen

Introduction

The origins of fractional calculus can be traced to a note from Leibuiz to L'Hospital 300 years ago, in which the meaning of the derivative of order one half is discussed.[1] Actually, fractional calculus derives from extending the derivatives and integrals of integer-order to noninteger cases. In the past few decades, many scholars have pointed out that derivatives and integrals of fractional order are highly suitable for the description of various physical objects, such as continuum mechanics, porous media, thermodynamics, electrodynamics, quantum mechanics, among others.[2] Recently, designing fractional-order controllers has become one of the most exciting topics in control theory. This idea was first proposed by Oustaloup.[3] He introduced a robust fractional-order control scheme called Common Robust d'Order Non-Entire.[4] Podlubny introduced the most well-known fractional-order proportion-integral-derivative controller, which is named $PI^{\lambda}D^{\mu}$.[5,6] Many additional fractional-order controllers have been proposed, including tilt-integral derivative (TID) controllers,[7] fractional-order lead–lag compensators,[8,9] fractional-order optimal controllers,[10,11] and fractional-order adaptive controllers.[12,13]

[1] College of Astronautics, Northwestern Polytechnical University, Xi'an, Shaanxi, People's Republic of China
[2] National Key Laboratory of Aerospace Flight Dynamics, Northwestern Polytechnical University, Xi'an, Shaanxi, People's Republic of China

Corresponding author:
Dong Zhang, College of Astronautics, Northwestern Polytechnical University, Xi'an, Shaanxi, 710072, People's Republic of China.
Email: zhangdong@nwpu.edu.cn

Sliding mode control (SMC) is a well-known effective control technique that is widely applied for both linear and nonlinear systems.[14] This control is also considered as a feasible control approach for systems with uncertainties. Generally, any linear sliding surface can guarantee the asymptotic stability and desired performance of the closed-loop control systems. However, monotonous switching feedback control gain causes the settling time of the closed-loop control system to increase, meaning that the system state cannot reach the equilibrium point in a finite time. Moreover, SMC offers high-frequency chattering of control input, which leads to undesirable loads on control actuators.

In recent years, with the development of fractional controls, many scholars have employed fractional-order SMC (FOSMC) to overcome these drawbacks. In the study of Dadras and Momeni[15], a novel type of control strategy called fractional-order terminal SMC (FO-TSMC) was introduced for a class of uncertain dynamical systems. Based on the Lyapunov stability theory, a fractional-order switching manifold was proposed to guarantee the sliding condition. The results of a simulation indicated that the proposed strategy ensured finite time stability for the closed-loop system. In the study of Mujumdar et al.,[16] an FOSMC scheme was proposed for control of a single-link flexible manipulator. The switching surface was constructed based on the fractional derivatives in the differential equation. The proposed FOSMC not only achieved better performance with small control chattering, but also was robust in the face of external load disturbance and parameter variations. In the study of Tang et al.,[17,18] the FOSMC was proposed for antilock braking systems (ABS) to regulate the slip to a desired value. These controllers not only deal with the uncertainties in ABS, but also track the desired slip faster than conventional integer-order SMC (IOSMC). Additionally, FOSMC has been employed for speed control of permanent magnet synchronous motors,[19,20] for vibration suppression of uncertain structures,[21] for control design of uncertain nonlinear systems,[22,23] for control of fractional-order chaotic systems,[24,25] and so on and achieved better control capacities.

To date, most of the research on FOSMC has focused on the fractional-order switching manifold, these FOSMC strategies improve the control capacities of conventional IOSMC by employing fractional-order switching manifold, but they cannot achieve optimal control performance without additional measures. In this article, an optimal FOSMC strategy is proposed for a class of uncertain nonlinear systems. The proposed control strategy is designed based on linear-quadratic optimal theory. Specially, a novel fractional-order sliding surface is introduced based on linear quadratic regulator (LQR). Therefore, the controller designed in this article is composed of two parts as nominal item and fractional item. The nominal item makes the system achieve convergence as quickly as possible and the fractional item rejects the system uncertainties to guarantee the necessary robustness. Finally, the stability of closed-loop system is proved by using Lyapunov stability theory.

The rest of this article is organized as follows. In section 2, some preliminaries and definitions of fractional calculus are introduced. In section 3, the uncertain nonlinear system and the tracking error dynamics are formulated. In section 4, the optimal FOSMC scheme based on LQR is constructed. Two academic examples are simulated in section 5. Finally, conclusions are included in section 6.

Basics definitions and preliminaries of fractional calculus

Definitions of fractional derivatives and integrals

Fractional calculus is a generalization of integration and differentiation to noninteger-order fundamental operator ${}_aD_t^\gamma$, where a and t are the bounds of the operation and $\gamma \in R$ is the fractional order.[26] The continuous integro-differential operator is defined as

$$ {}_aD_t^\gamma = \begin{cases} \dfrac{d^\gamma}{dt^\gamma}, & \gamma > 0, \\ 1, & \gamma = 0, \\ \int_a^t (d\tau)^\gamma, & \gamma < 0, \end{cases} \tag{1} $$

There are three commonly used definitions for fractional derivatives involving Grünwald–Letnikov (GL), Riemann–Liouville (RL), and Caputo definitions. The GL definition is

$$ {}_aD_t^\gamma f(t) = \lim_{h \to 0} h^{-\gamma} \sum_{j=0}^{[(t-a)/h]} (-1)^j \binom{\gamma}{j} f(t - jh) \tag{2} $$

where h is the time increment, $[x]$ means the nearest integer no more than x, and

$$ \binom{\gamma}{j} = \frac{\Gamma(\gamma + 1)}{\Gamma(j+1)\Gamma(\gamma - j + 1)} \tag{3} $$

with *Gamma* function $\Gamma(\cdot)$. The RL definition is

$$ {}_aD_t^\gamma f(t) = \frac{1}{\Gamma(n-\gamma)} \frac{d^n}{dt^n} \int_a^t \frac{f(\tau)}{(t-\tau)^{\gamma - n + 1}} d\tau \ \text{ for } n - 1 < \gamma < n \tag{4} $$

The Caputo definition is given by

$$ {}_aD_t^\gamma f(t) = \frac{1}{\Gamma(n-\gamma)} \int_a^t \frac{f^{(n)}(\tau)}{(t-\tau)^{\gamma - n + 1}} \, \mathrm{d}\tau \ \text{ for } n - 1 < \gamma < n \tag{5} $$

As mentioned above, under the homogenous initial conditions, the RL and the Caputo derivatives are equivalent.

Approximation of fractional derivative

Recall the approximate GL definition given below, where the step size of h is assumed to be very small

$$
\begin{aligned}
{}_aD_t^{\gamma} f(t) &\approx h^{-\gamma} \sum_{j=0}^{[(t-a)/h]} (-1)^j \binom{\gamma}{j} f(t-jh) \\
&= h^{-\gamma} \sum_{j=0}^{[(t-a)/h]} \omega_j f(t-jh)\,, \qquad (6)
\end{aligned}
$$

where the binomial coefficients can recursively be calculated with the following formula

$$
\omega_0 = 1, \omega_j = \left(1 - \frac{\gamma+1}{j}\right)\omega_{j-1}, j = 1, 2, \cdots. \qquad (7)
$$

This approximation method is very satisfied when $|\gamma| < 1$[27] For the case $|\gamma| > 1$, it is usual to split fractional operator like

$$
{}_aD_t^{\gamma} = {}_aD_t^{n}({}_aD_t^{\delta}),\ \ \gamma = n + \delta,\ \ n \in Z,\ \ \delta \in [0, 1] \qquad (8)
$$

Then, only the term of ${}_aD_t^{\delta}$ need to be approximated.

Problem statement

Consider an uncertain affine nonlinear system of the form

$$
\begin{cases} \dot{x} = f(x) + g(x)u \\ y = H(x) \end{cases} \qquad (9)
$$

where $x \in R^n$ and $u \in R^m$ are the state variable and control input, respectively, and $y \in R^m$ is the system output. $f(x) = [f_1(x) \ \cdots \ f_n(x)]^T$ and $g(x) = [g_1(x) \ \cdots \ g_m(x)]$ are the smooth uncertain functions including inertial parameter uncertainties and external disturbances. $H(x) = [h_1(x) \ \cdots \ h_m(x)]^T$ is the measureable smooth output function. While the relative degree $r_i (i = 1, \ldots, m)$ of the system with respect to the system outputs is constant and known. The solutions are understood in the Filippov sense,[28] and system trajectories are supposed to be infinitely extendible in time for any bounded Lebesgue-measurable input.

The control task is to track the reference command $y_d \in R^m$ with tracking error $e(x) = [e_1(x) \ \cdots \ e_m(x)]^T = y_d(x) - y(x)$ converges to $e = 0$ in finite time. To achieve this control object, by using the technique of input/output feedback linearization, system (9) is linearized to be decoupled tracking error dynamics as follows.

After differentiating r_i times of each tracking error element e_i, the tracking error dynamics can be presented as

$$
\begin{aligned}
e^{[r]} &= \begin{bmatrix} e_1^{(r_1)} \\ e_2^{(r_2)} \\ \vdots \\ e_m^{(r_m)} \end{bmatrix} = \begin{bmatrix} L_f^{r_1} e_1 \\ L_f^{r_2} e_2 \\ \vdots \\ L_f^{r_m} e_m \end{bmatrix} \\
&+ \begin{bmatrix} L_{g_1} L_{f_0}^{r_1-1} e_1 & L_{g_2} L_f^{r_1-1} e_1 & \cdots & L_{g_m} L_f^{r_1-1} e_1 \\ L_{g_1} L_{f_0}^{r_2-1} e_2 & L_{g_2} L_f^{r_2-1} e_2 & \cdots & L_{g_m} L_f^{r_2-1} e_2 \\ \cdots & \cdots & \cdots & \cdots \\ L_{g_1} L_f^{r_m-1} e_m & L_{g_2} L_f^{r_m-1} e_m & \cdots & L_{g_m} L_f^{r_m-1} e_m \end{bmatrix} u
\end{aligned} \qquad (10)
$$

or

$$
e^{[r]} = F^*(x) + G^*(x)u \qquad (11)
$$

where $r = (r_1, r_2, \ldots, r_m)$ is the vector of relative degree.

Due to existences of the system uncertainty, equation (11) can be rewritten as the form

$$
e^{[r]} = F_0^*(x) + G_0^*(x)u + d(x) \qquad (12)
$$

where $F_0^*(x)$ and $G_0^*(x)$ are the nominal items derived from the known parts of $f(x)$ and $g(x)$. While $G_0^*(x)$ is assumed to be nonsingular when $t > 0$. $\mathrm{d}(x)$ presents the unknown lumped uncertainty and is assumed to be boundable.[29]

Furthermore, if $\sum_{i=1}^{m} r_i = n$, the dynamic equations of the tracking error system are decoupled into canonical forms as

$$
\begin{cases} \dot{\varsigma}_1^i = \varsigma_2^i \\ \dot{\varsigma}_2^i = \varsigma_3^i \\ \vdots \\ \dot{\varsigma}_{r_i}^i = L_{f_0}^{r_i} e_i + \sum_{j=1}^{m} L_{g_{0j}} (L_{f_0}^{r_i-1} e_i) u_j + d(x)_i = v_i - d_i(x) \end{cases} \qquad (13)
$$

where $\varsigma_{r_i}^i = e_i^{(r_i-1)} = L_{f_0}^{r_i-1} e_i$, f_0 and g_{0j} are the nominal portions of $f(x)$ and $g(x)$ respectively, v_i is the ith element of v, $d_i(x)$ is the ith element of $d(x)$, and $i = 1, 2, \ldots, m$, $j = 1, 2, \ldots, m$.

FOSMC based on LQR

For stabilizing system (13), when there are no uncertainties, LQR is designed to guarantee the finite time convergence of the tracking error dynamics. In classical linear control theories, LQR is an optimal controller derived from solving linear-quadratic optimization problems. It has shown excellent performance in the control synthesis of linear systems. However, if unmodeled dynamics and system uncertainties are taken into account, it will be difficult to guarantee the control objective with LQR alone. Thus, in this section, a novel optimal FOSMC strategy is designed based on LQR to counteract the inertial uncertainties. Compared to conventional IOSMC, the magnitude of control chattering is drastically depressed.

Therefore, to stabilize system (13) in finite time, the auxiliary control input v_i is composed of two parts

$$
v_i = v_n + v_s \qquad (14)
$$

where the first item v_n, named nominal control, is continuous and stabilizes system (13) as soon as possible when there are no uncertainties. And the second item v_s, named fractional control, is discontinuous and conquers uncertainty to guarantee system robustness and ensures that control objectives are reached.

Nominal control based on LQR (v_n)

Consider the particular case $d_i(x) = 0$. Then, there is no need to compensate the uncertainties, the control law reads as $v_i = v_n$. Therefore, system (13) is rewritten as a linear form of

$$\dot{z} = A \cdot z + B \cdot v_n \tag{15}$$

where $z = [\varsigma_1^i \quad \cdots \quad \varsigma_{r_i}^i]^T$. A and B are defined by

$$A = \begin{bmatrix} 0 & 1 & 0 & \cdots & 0 \\ 0 & 0 & 1 & \cdots & 0 \\ \vdots & \vdots & \vdots & \ddots & \vdots \\ 0 & 0 & 0 & \cdots & 1 \\ 0 & 0 & 0 & \cdots & 0 \end{bmatrix}_{r_i \times r_i}, \quad B = \begin{bmatrix} 0 \\ \vdots \\ 0 \\ 1 \end{bmatrix}_{r_i \times 1}$$

The control objective is to drive the state of system (15) to $z = 0$ as soon as possible. This objective can be achieved through the use of linear optimal control theory. In this article, we design continuous control input v_n by linear-quadratic optimal control laws. Considering intermediate objective function

$$J = \frac{1}{2}\int_0^\infty (z^T Q z + \alpha v_n^2) dt, \ (Q \in R^{r_i \times r_i}, \alpha \in R) \tag{16}$$

the control input v_n is derived by minimizing J subjected to (16)

$$v_n = -\alpha^{-1} B^T P z \tag{17}$$

where P is the positive-definite solution to the Riccati equation with design parameters Q and a

$$A^T P + PA - \alpha^{-1} P B^T B P + Q = 0, \ (Q, \alpha > 0) \tag{18}$$

Obviously, it can be easily verified that if $d_i(x) \neq 0$, system (13) will not converge to the origin in finite time under the control law (17).

Fractional control (v_s)

As mentioned above, finite time convergence cannot be guaranteed when system uncertainties exist in system (13). Therefore, fractional control item is employed as one of the integrated control to achieve robustness. Then, the closed-loop system can reject system uncertainties, and the control input is chattering reduced.

Generally, conventional IOSMC employs the sliding surface that is linear, stable differential operator on the tracking error.[29] Thus, the conventional sliding surface gets the form as

$$\sigma_c = \left(\frac{d}{dt} + \lambda\right)^{r_i - 1} e_i \tag{19}$$

where λ defines the bandwidth of the tracking error dynamics.

Based on the conventional sliding surface σ_c, we define a fractional-order sliding surface as the following form

$$\begin{cases} \sigma = \left(\frac{d}{dt} + \lambda_1\right)^{r_i - 1} e_i - \left(\frac{d}{dt} + \lambda_2\right)^{r_i - 2} D^\eta e_i + v_{\text{aux}} \\ \dot{v}_{\text{aux}} = -v_n \end{cases} \tag{20}$$

Compared to conventional sliding surface σ_c, a fractional item $\left(\frac{d}{dt} + \lambda_2\right)^{r_i - 2} D^\eta e_i$ and an auxiliary item v_{aux} are adopted.

Then differentiating the fractional-order sliding surface in (20), we have

$$\dot{\sigma} = e_i^{(r_i)} + \sum_{j=1}^{r_i - 1} b_j e_i^{(j)} - \sum_{j=0}^{r_i - 2} c_j D^{\eta + j} e_i - v_n \tag{21}$$

Combining (12) with (21), we obtain

$$\begin{aligned} \dot{\sigma} &= \sum_{j=1}^{r_i - 1} b_j e_i^{(j)} - \sum_{j=0}^{r_i - 2} c_j D^{\eta + j} e_i + v_i - d_i(x) - v_n \\ &= \sum_{j=1}^{r_i - 1} b_j e_i^{(j)} - \sum_{j=0}^{r_i - 2} c_j D^{\eta + j} e_i + v_s - d_i(x) \end{aligned} \tag{22}$$

where $b_j = \begin{bmatrix} r_i - 1 \\ j - 1 \end{bmatrix} \frac{(r_i - 1)! \lambda_1^{r_i - j}}{(r_i - j)!(j - 1)!}$ and $c_j = \begin{bmatrix} r_i - 2 \\ j - 1 \end{bmatrix} \frac{(r_i - 2)! \lambda_2^{r_i - 1 - j}}{(r_i - 1 - j)!(j - 1)!}$.

Let $\dot{\sigma} = 0$, the discontinuous controller is obtained as follows

$$v_s = -\sum_{j=1}^{r-1} b_j e_i^{(j)} + \sum_{j=0}^{r-2} c_j D^{\eta + j} e_i - k_i \operatorname{sgn}(\sigma) \tag{23}$$

where k_i is a switching feedback control gain and might be any positive number. In (23), the first-order SMC item $k_i \operatorname{sgn}(\sigma)$ (with $k_i > |d_i(x)|$) is considered as the equivalent control part to reject the system uncertainty. When system (13) evolves on the sliding mode $\sigma = 0$, the equivalent control part can be gotten the form as $k_i \operatorname{sgn}(\sigma) = d_i(x)$. And $\operatorname{sgn}(\cdot)$ is sign function as

$$\operatorname{sgn}(\sigma) = \begin{cases} -1, & \sigma < 0 \\ 0, & \sigma = 0 \\ 1, & \sigma > 0 \end{cases} \tag{24}$$

Lyapunov stability analysis

Lyapunov stability analysis is a common approach to deal with the stability problem of linear/nonlinear systems. Thus, this part employs Lyapunov stability theory to prove the finite time convergence of the sliding motion and the global stability of the closed-loop control system as follows.

Theorem. Considering the tacking error dynamics of system (13), if it is controlled with the fractional sliding mode controlling law described by $v_i = v_n + v_s$, where v_n and v_i are defined by (17) and (23), respectively, then the tracking error trajectory will converge to the proposed sliding surface (20) in finite time.

Proof. Choosing the Lyapunov function as

$$V = |\sigma| \tag{25}$$

Differentiating equation (25), we obtain

$$\dot{V} = \dot{\sigma}\,\mathrm{sgn}(\sigma) = \left(v_s + \sum_{j=1}^{r-1} c_j e^{(j)} - \sum_{j=0}^{r-2} d_j D^{\eta+j} e\right) \mathrm{sgn}(\sigma) \tag{26}$$

Substituting (23) into (26), we obtain

$$\dot{V} = -k_i[\,\mathrm{sgn}(\sigma)]^2 \le 0 \tag{27}$$

Therefore, on the basis of Lyapunov stability theorem, the state variables of the closed-loop control system will converge to the equilibrium point.

Before the sliding motion is stable, $[\,\mathrm{sgn}(\sigma)]^2 = 1$ always holds true. Thus, equation (27) is rewritten as the following form

$$\dot{V} = \frac{d|\sigma|}{dt} = -k_i \tag{28}$$

Then, we obtain

$$dt = \frac{d|\sigma|}{-k_i} \tag{29}$$

The sliding motion happens within finite time, then we taking integral of both sides of (29) from 0 to t_r

$$\int_0^{t_r} dt = -\frac{1}{k_i}\int_{|\sigma(0)|}^{|\sigma(t_r)|} dt \tag{30}$$

Set $\sigma(t_r) = 0$, we obtained that

$$t_r = -\frac{|\sigma|}{k_i}\Big|_{|\sigma(0)|}^{|\sigma(t_r)|} = \frac{|\sigma(0)|}{k_i} \tag{31}$$

Therefore, the tracking error trajectory of system (13) will converge to the sliding surface $\sigma = 0$ within the finite time $t_r = \frac{|\sigma(0)|}{k_i}$, and the proof has been completed.

Remark. As mentioned in Utkin,[30] non-smooth Lyapunov functions can be applied to check the finite time convergence of a system. Therefore, choosing the non-smooth Lyapunov function $V = |\sigma|$ is common in the literatures.[17,21,31]

Simulation examples

A kinematic model of a car

The control of a kinematic model of a car is illustrated in this part. It has been chosen to test the performances of sliding mode algorithms.[32–34] The system is described by

$$\begin{cases} \begin{bmatrix} \dot{x}_1 \\ \dot{x}_2 \\ \dot{x}_3 \\ \dot{x}_4 \end{bmatrix} = \begin{bmatrix} w\cos(x_3) \\ w\sin(x_3) \\ w\tan(x_4)/L \\ 0 \end{bmatrix} + \begin{bmatrix} 0 \\ 0 \\ 0 \\ 1 \end{bmatrix} u \\ y = x_2 \end{cases} \tag{32}$$

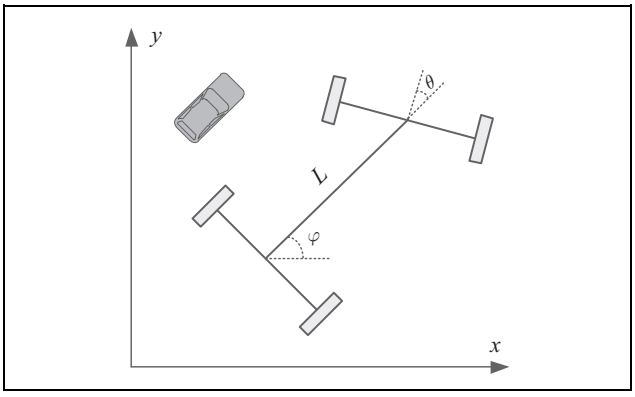

Figure 1. Kinematic car model.

where (x_1, x_2) are the Cartesian coordinates of the rear-axle middle point, x_3 is the orientation angle, x_4 is the steering angle, and u is the control variable (Figure 1). w is the longitudinal velocity ($w = 10$ m/s), and L is the length between the two axles ($L = 5$ m). The velocity is assumed to be known with $\delta w = 5\%$ of uncertainty ($w = 10 \times (1 \pm 5\%)$ m/s). The control objective is to steer the car from a given initial position to the reference trajectory $y_{\mathrm{ref}} = 10\sin(0.05x_1) + 5$ in finite time. Thus, the tracking error is expressed as

$$e = x_2 - 10\sin(0.05x_1) - 5 \tag{33}$$

The relative degree of system (32) is easy to be calculated as 3

$$\dot{e} = \frac{w}{2}\cos\left(\frac{x_1}{20}\right)\cos(x_3) - w\sin(x_3),$$

$$\ddot{e} = -\frac{w^2}{L}\cos(x_3)\tan(x_4) - \frac{w^2}{40}\sin\left(\frac{x_1}{20}\right)\cos^2(x_3) - \frac{w^2}{2L}\cos\left(\frac{x_1}{20}\right)\sin(x_3)\tan(x_4),$$

$$\dddot{e} = -u\cdot\frac{w^2}{L}\sec^2(x_4)\left(\cos(x_3) + \frac{1}{2}\cos\left(\frac{x_1}{20}\right)\sin(x_3)\right) - \frac{w^3}{L^2}\tan^2(x_4)\left(\frac{1}{2}\cos\left(\frac{x_1}{20}\right)\cos(x_3) - \sin(x_3)\right) + \frac{3w^3}{40L}\sin\left(\frac{x_1}{20}\right)\cos(x_3)\sin(x_3)\tan(x_4) - \frac{w^3}{800}\cos\left(\frac{x_1}{20}\right)\cos^3(x_3)$$

Then, we obtain

$$\dddot{e} = f^*(x) + g^*(x)\cdot u = v$$

where $x = [\,x_1 \;\; x_2 \;\; x_3 \;\; x_4\,]^T$ is the state vector of system (32).

Let $z = [\,e \;\; \dot{e} \;\; \ddot{e}\,]^T$. Then, the tracking error dynamics of system (32) is described as

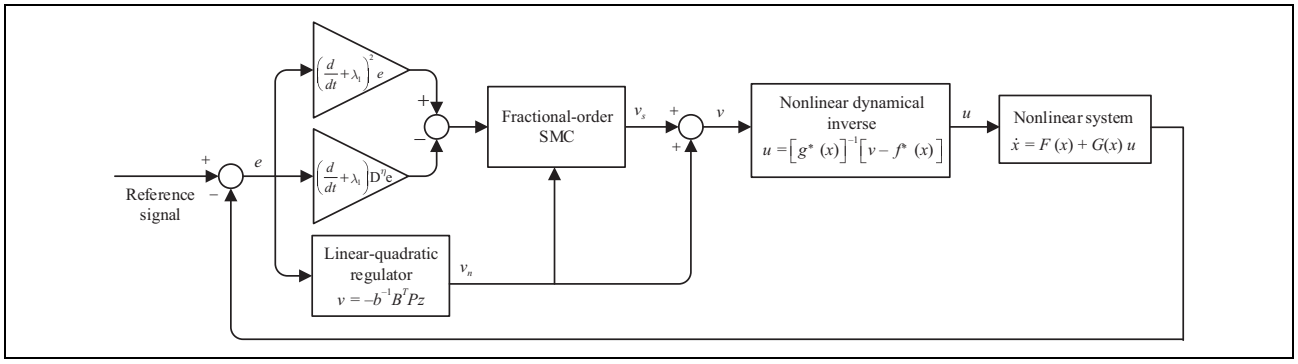

Figure 2. Block diagram of the fractional-order control system.

$$\dot{z} = \begin{bmatrix} 0 & 1 & 0 \\ 0 & 0 & 1 \\ 0 & 0 & 0 \end{bmatrix} z + \begin{bmatrix} 0 \\ 0 \\ 1 \end{bmatrix} v$$

where $v = v_n + v_s$.

First, the continuous control part v_n is derived by solving the Riccati equation (18) for a positive matrix Q and a positive number b. The solution of this equation, P, is a symmetric positive definite matrix. Matrix Q and number b are stated as

$$Q = \begin{bmatrix} 5 & 0 & 0 \\ 0 & 1 & 0 \\ 0 & 0 & 1 \end{bmatrix}, \ \alpha = 2$$

Then, P is calculated as

$$P = \begin{bmatrix} 9.1896 & 7.9448 & 3.1623 \\ 7.9448 & 11.4396 & 5.8120 \\ 3.1623 & 5.8120 & 5.0247 \end{bmatrix}$$

Second, the fractional control part v_s is obtained by assigning the fractional-order sliding surface as $\sigma_1 = \left(\frac{d}{dt} + \lambda_1\right)^2 e - \left(\frac{d}{dt} + \lambda_2\right) D^\eta e + v_{aux}, \dot{v}_{aux} = -v_n$. Then, the nonlinear controller proposed in this article (denoted as FOSMC-LQR) is constructed as

$$u = \frac{1}{g^*(x)} \Big(- b^{-1} B^T Pz - 2\lambda_1 \ddot{e} - \lambda_1^2 \dot{e} + D^{\eta+2} e + \lambda_2 D^{\eta+1} e - k_1 \operatorname{sgn}(\sigma_1) - f^*(x) \Big).$$

The block diagram of the fractional-order control system is shown in Figure 2. For comparison, there are another three different controllers to be considered: a conventional IOSMC, a conventional IOSMC based on LQR (denoted as IOSMC-LQR), and a single FOSMC. These three controllers are formulated as following expressions

The IOSMC is

$$u = \frac{1}{g^*(x)} \Big(- 2\lambda_1 \ddot{e} - \lambda_1^2 \dot{e} - k_2 \operatorname{sgn}(\sigma_2) - f^*(x) \Big)$$

where integer-order sliding surface $\sigma_2 = \left(\frac{d}{dt} + \lambda\right)^2 e$.

The IOSMC-LQR is

$$u = \frac{1}{g^*(x)} \Big(- b^{-1} B^T Pz - 2\lambda_1 \ddot{e} - \lambda_1^2 \dot{e} - k_3 \operatorname{sgn}(\sigma_2) - f^*(x) \Big)$$

And the single FOSMC is

$$u = \frac{1}{g^*(x)} \Big(- 2\lambda_1 \ddot{e} - \lambda_1^2 \dot{e} + D^{\eta+2} e + \lambda_2 D^{\eta+1} e - k_4 \operatorname{sgn}(\sigma_1) - f^*(x) \Big)$$

In simulations, the design parameters of the three aforementioned controllers are given the values as ($\lambda_1 = 0.5$, $\lambda_2 = -0.8$, $\eta = 0.2$, $k_1 = 0.8$, $k_2 = 5$, $k_3 = 5$, $k_4 = 5$). Then, the simulation results and their analysis are illustrated as follows.

Figure 3 displays a comparison of the system response between the single LQR and the proposed controller in this article (FOSMC-LQR). It can be clearly seen that single LQR results in an unsteady tracking trajectory, and the tracking error oscillates up and down around $e = 0$. In contrast, the system response with FOSMC-LQR presents a better tracking trajectory, and its tracking error achieves convergence in finite time.

Figure 4 gives a system response comparison of the single FOSMC and the FOSMC-LQR. As shown in the figures, single FOSMC requires larger switching feedback control gain, $k_4 = 5$ compared to $k_1 = 0.8$, to reject the system uncertainty. Because of the larger value of the switching feedback control gain, the control input of the single FOSMC shows a higher chattering magnitude. As shown in Figure 4(c) and (d), the system response with FOSMC-LQR presents faster convergence velocities of the tracking error and the sliding motion.

The integer-order and fractional-order derivatives of the tracking error are demonstrated in Figure 5, such as $(e, \dot{e}, \ddot{e})$ in Figure 5(a) and $(D^{0.2}e, D^{1.2}e, D^{2.2}e)$ in Figure 5(b). Compared to conventional IOSMC, FOSMC adopts extra fractional-order derivatives of the tracking error, as $\left(\frac{d}{dt} + \lambda_2\right)^{r-2} D^\eta e$ in (25). This causes the sliding motion of FOSMT to converge to $\sigma = 0$ faster. Figure 6 shows the

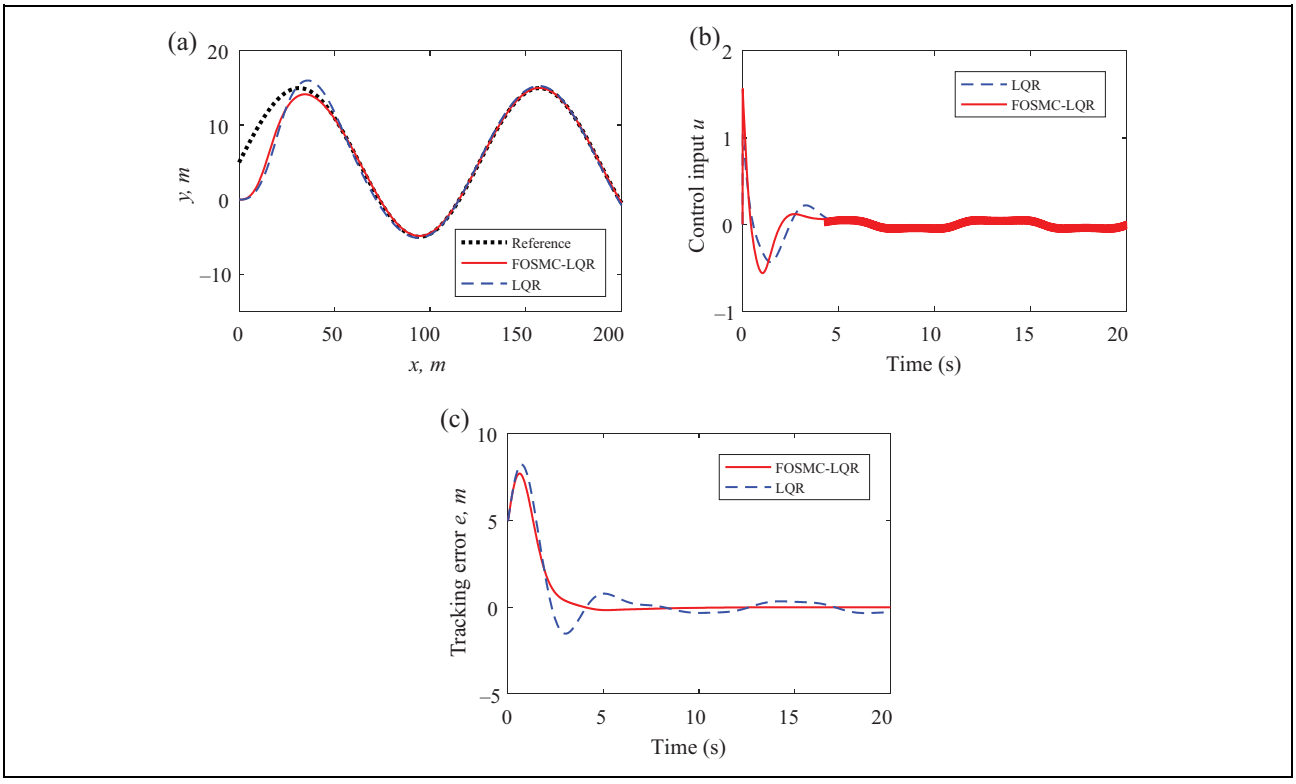

Figure 3. Comparison of system response between LQR and FOSMC-LQR. LQR: linear-quadratic regulator; FOSMC: fractional-order sliding mode control.

comparison of system response between conventional IOSMC and FOSMC. As shown in the figures, FOSMC presents smaller tracking error and faster convergence velocity in the sliding motion. Therefore, fractional-order derivatives of the tracking error are necessary for the improvement of control performance.

Figure 7 shows a system response comparison between IOSMC-LQR and FOSMC-LQR. As the figures show, FOSMC-LQR can achieve steady tracking performance with small switching feedback control gain because it adopts extra fractional-order derivatives of the tracking error. On the other hand, to ensure the similar control performance, IOSMC-LQR requires a larger switching feedback control gain, which leads to a higher magnitude of control chattering and fierce oscillation of the sliding motion.

Under the conditions of $\lambda_2 = 0.8$ and $\lambda_2 = -0.8$, the system responses of FOSMC-LQR with different fractional orders (as η approaches the values of 0.2, 0.5, and 0.8) are shown in Figures 8 and 9. As shown in the figures, when $\lambda_2 = -0.8$ and $\eta = 0.2$, the FOSMC-LQR presents better performance in tracking trajectory, faster convergence of tracking error, and lower amplitude of sliding motion. However, when $\lambda_2 = 0.8$, the FOSMC-LQR with $\eta = 0.8$ presents better control performance than that with $\eta = 0.2$. It can be seen that the fractional order η and the weight λ_2 of fractional-order derivatives affected the controller capacities synthetically. Therefore, to obtain a desirable control performance, the tradeoff between η and λ_2 should be considered in practical applications.

A dynamic model of a two-link rigid robot manipulator

The physical model of a two-link rigid robot that moves a horizontal plane is shown in Figure 10. Each joint is equipped with a motor for providing input torque, an encoder for measuring joint position, and a tachometer for measuring joint velocity. The objective of control design is to make the joint position q_1 and q_2 follow desired position histories $q_{d1}(t)$ and $q_{d2}(t)$, which are specified by the motion planning system of the robot. Such tracking control problems arise when a robot hand is required to move along a specified path, for example, to draw circles.[35,36]

By using Lagrangian equations in classical dynamics, the differential equations of the robot are expressed as

$$\dot{q}_1 = \omega_1, \quad \dot{q}_2 = \omega_2,$$
$$\begin{bmatrix} \dot{\omega}_1 \\ \dot{\omega}_2 \end{bmatrix} = M^{-1}\left\{ \begin{bmatrix} u_1 \\ u_2 \end{bmatrix} - \begin{bmatrix} -p\omega_2 & -p(\omega_1+\omega_2) \\ p\omega_1 & 0 \end{bmatrix} \begin{bmatrix} \omega_1 \\ \omega_2 \end{bmatrix} \right\}. \tag{34}$$

where

$$M = \begin{bmatrix} M_{11} & M_{12} \\ M_{21} & M_{22} \end{bmatrix}$$

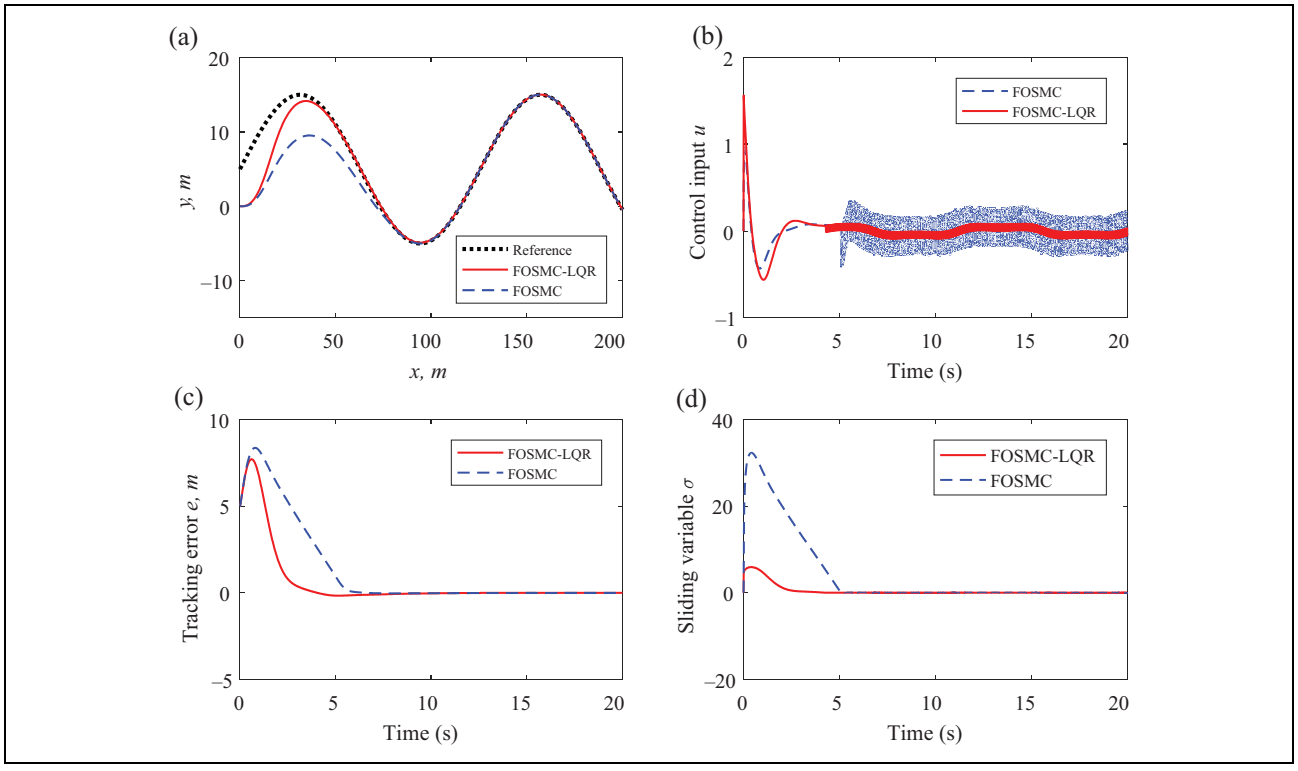

Figure 4. Comparison of system response between FOSMC and FOSMC-LQR. LQR: linear-quadratic regulator; FOSMC: fractional-order sliding mode control.

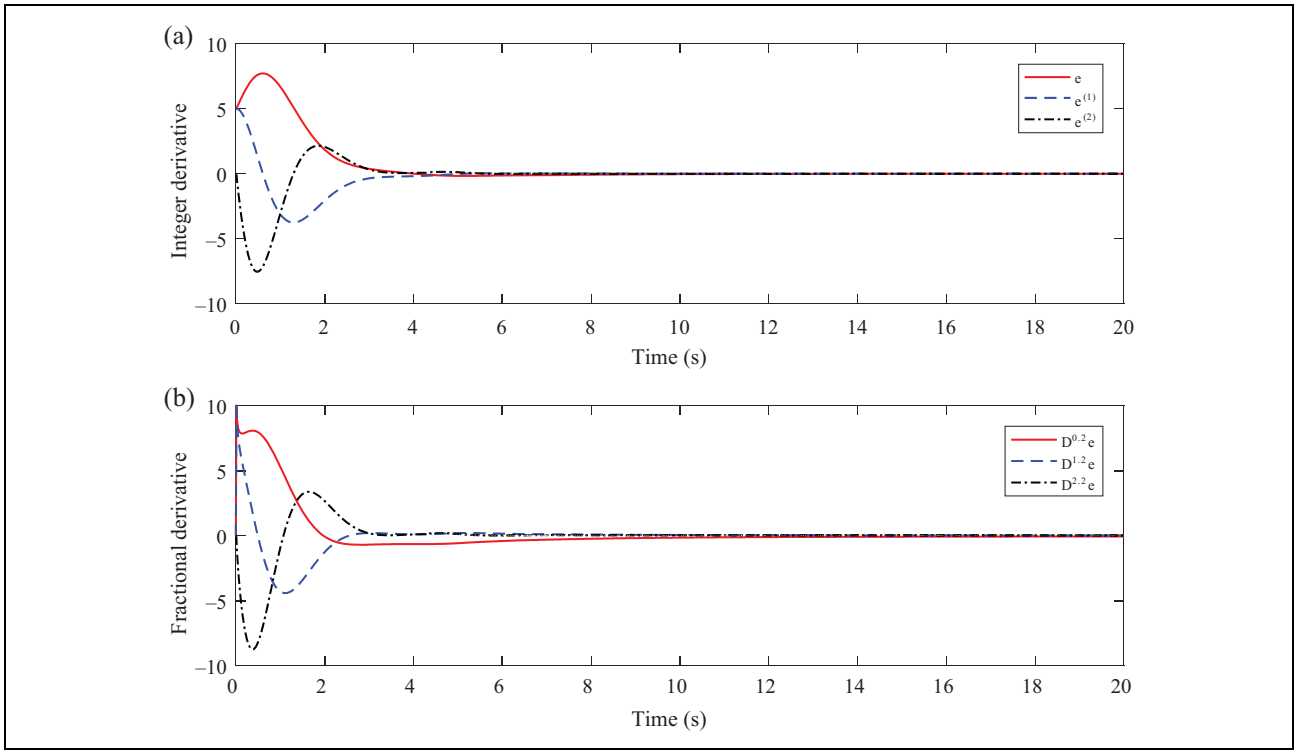

Figure 5. Integer- and fractional-order derivatives of the tracking error.

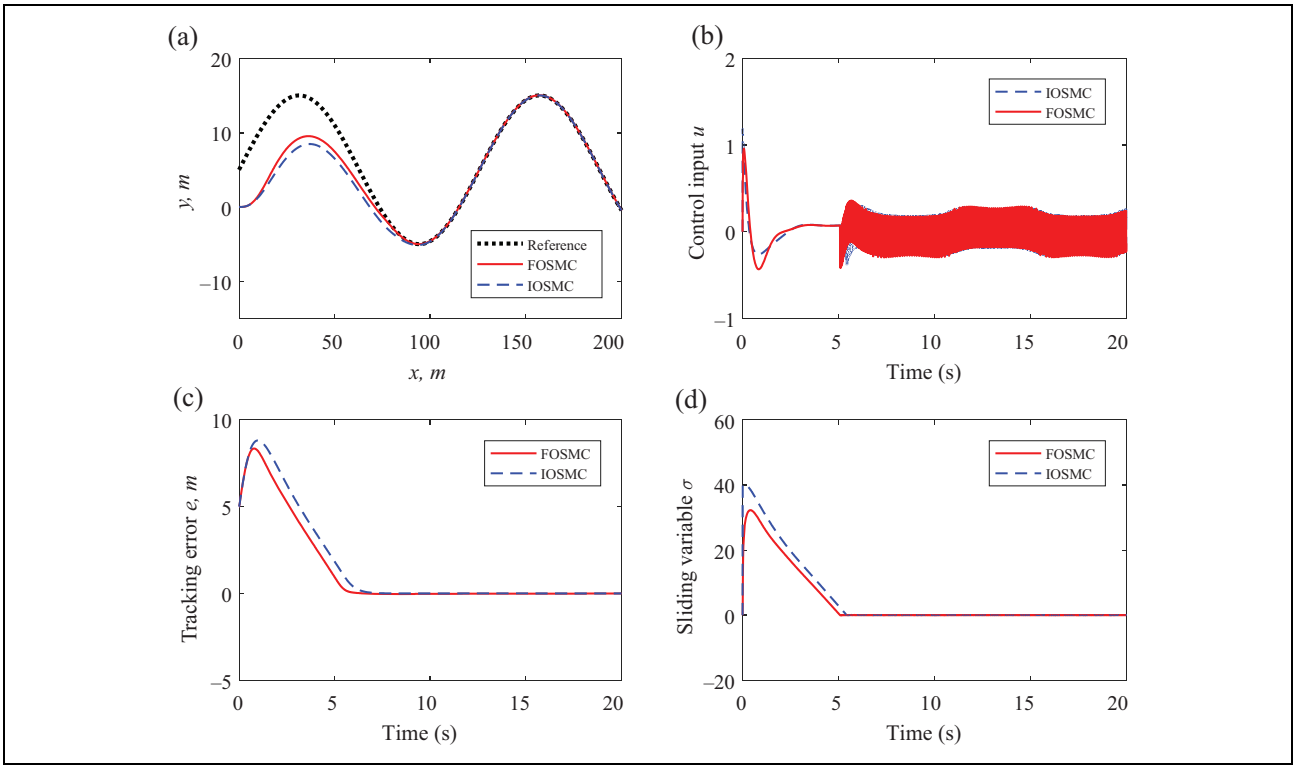

Figure 6. Comparison of system response between IOSMC and FOSMC. IOSMC: integer-order sliding mode control; FOSMC: fractional-order sliding mode control.

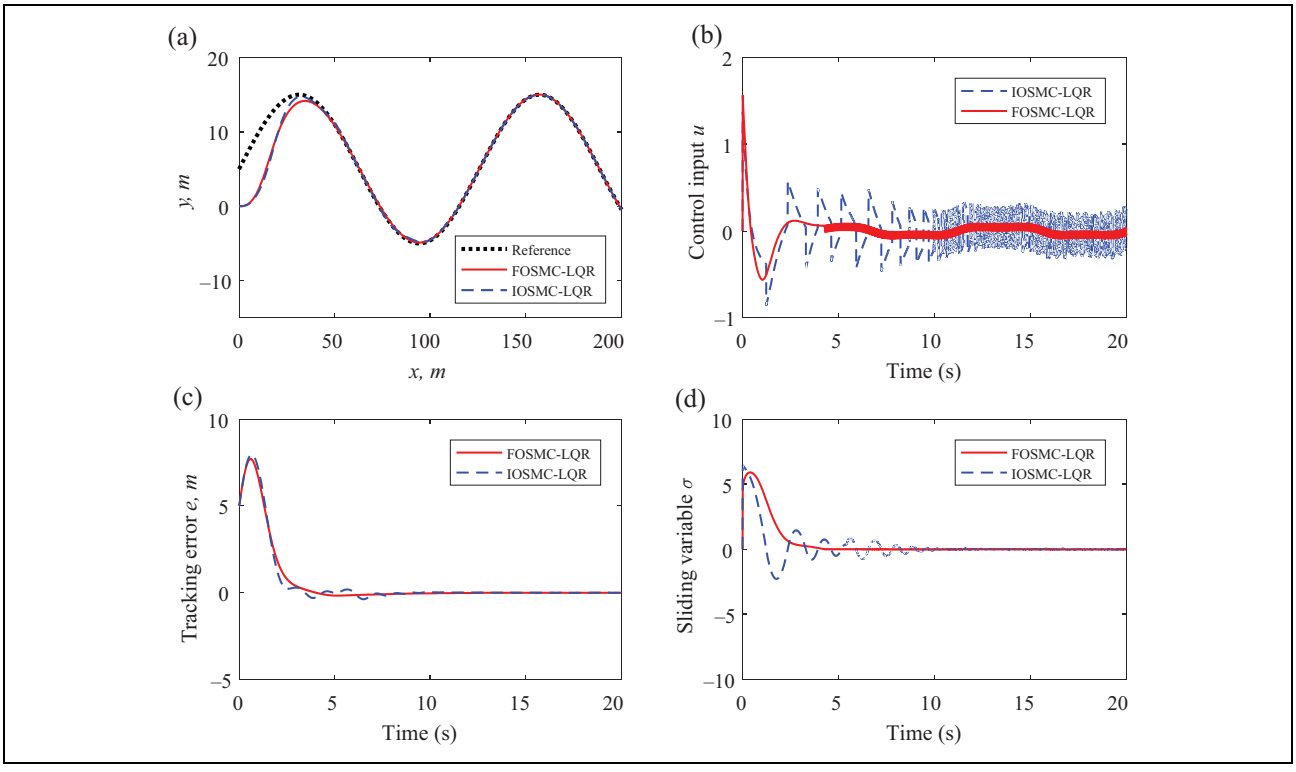

Figure 7. Comparison of system response between IOSMC-LQR and FOSMC-LQR. IOSMC: integer-order sliding mode control; LQR: linear-quadratic regulator; FOSMC: fractional-order sliding mode control.

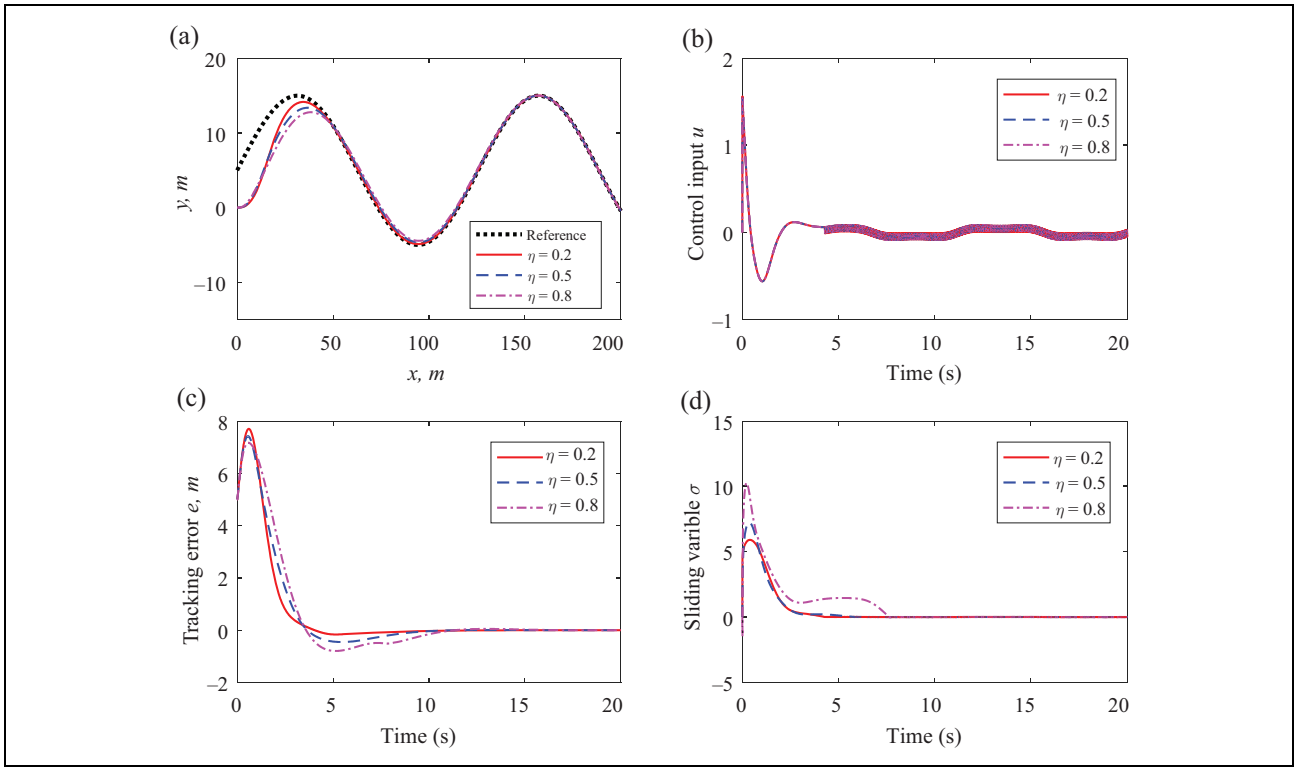

Figure 8. When $\lambda_2 = -0.8$, system responses of FOSMC-LQR with different fractional-order η. LQR: linear-quadratic regulator; FOSMC: fractional-order sliding mode control.

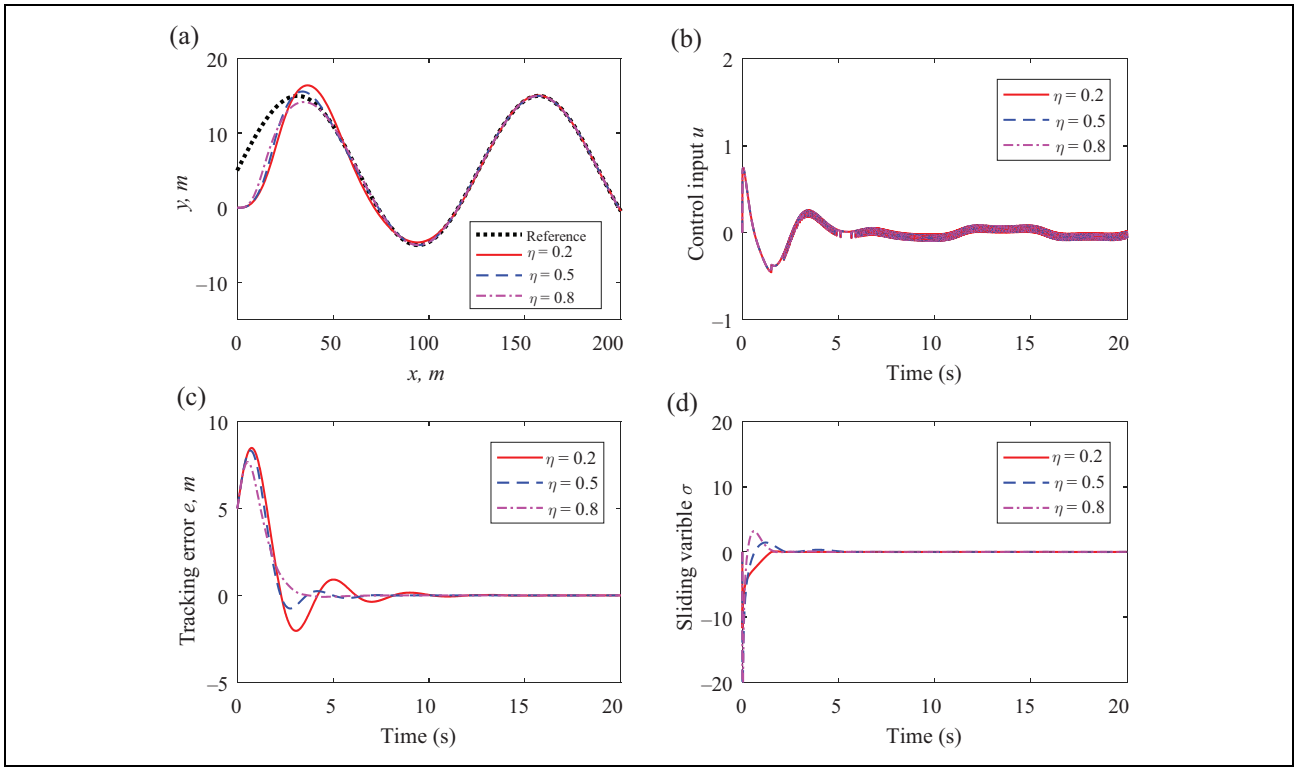

Figure 9. When $\lambda_2 = 0.8$, system responses of FOSMC-LQR with different fractional-order η. LQR: linear-quadratic regulator; FOSMC: fractional-order sliding mode control.

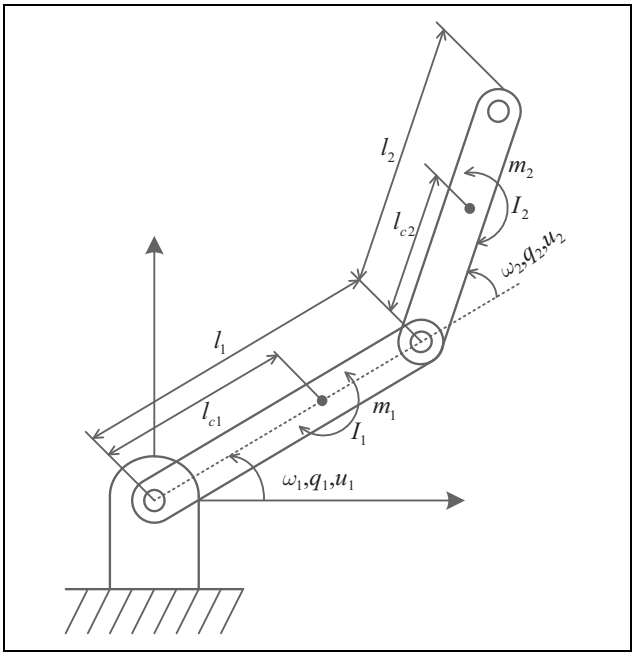

Figure 10. A two-link robot.

$$
\begin{aligned}
M_{11} &= a_1 + 2a_3\cos(q_2) + 2a_4\sin(q_2)\\
M_{22} &= a_2\\
M_{12} &= M_{21} = a_2 + a_3\cos(q_2) + a_4\sin(q_2)\\
p &= a_3\sin(q_2) - a_4\cos(q_2)\\
a_1 &= I_1 + m_1 l_{c1}^2 + I_2 + m_2 l_{c2}^2 + m_2 l_1^2\\
a_2 &= I_2 + m_2 l_{c2}^2\\
a_3 &= m_2 l_1 l_{c2}\cos(\delta_e)\\
a_4 &= m_2 l_1 l_{c2}\sin(\delta_e)
\end{aligned}
$$

In real physical systems, the aforementioned constant parameters are always measured with inertial uncertainties. In this article, all of the parameter uncertainties are assumed as an additive variance to the nominal values. The nominal parameters are defined as[28]

$$
\begin{aligned}
&l_1^0 = 1.0, \quad l_{c1}^0 = 0.5, \quad m_1^0 = 1.0, \quad I_1^0 = 0.12,\\
&\delta_e^0 = 30^\circ, \quad l_{c2}^0 = 0.6, \quad m_2^0 = 2.0, \quad I_2^0 = 0.25
\end{aligned}
$$

And the uncertain parameters are calculated as

$$
\begin{aligned}
&l_1 = l_1^0 + \Delta l_1, \quad l_{c1} = l_{c1}^0 + \Delta l_{c1}, \quad m_1 = m_1^0 + \Delta l_{c1}, \quad I_1 = I_1^0 + \Delta I_1,\\
&\delta_e = \delta_e^0 + \Delta\delta_e, \quad l_{c2} = l_{c2}^0 + \Delta l_{c2}, \quad m_2 = m_2^0 + \Delta m_2, \quad I_2 = I_2^0 + \Delta I_2
\end{aligned}
\tag{35}
$$

where the additive variances (Δ) are parameter uncertainties, which are assigned as

$$
\begin{aligned}
&\Delta l_1 = 15\%l_1^0\cdot\sin(2t), \quad \Delta l_{c1} = 15\%l_{c1}^0\cdot\sin(2t),\\
&\Delta m_1 = 15\%m_1^0\cdot\cos(2t), \quad \Delta I_1 = 15\%I_1^0\cdot\sin(3t),\\
&\Delta\delta_e = 15\%\delta_e^0\cdot\cos(3t), \quad \Delta l_{c2} = 15\%l_{c2}^0\cdot\sin(2t),\\
&\Delta m_2 = 15\%m_2^0\cdot\cos(2t), \quad \Delta I_2 = 15\%I_2^0\cdot\sin(3t)
\end{aligned}
\tag{36}
$$

Let $x = [q_1 \;\; q_2 \;\; \omega_1 \;\; \omega_2]^T$, $y = [y_1 \;\; y_2]^T = [q_1 \;\; q_2]^T$, $u = [u_1 \;\; u_2]^T$, and

$$
g(x) = \begin{bmatrix} 0_{2\times 2} \\ M^{-1} \end{bmatrix}_{4\times 2},
$$

$$
f(x) = \begin{bmatrix} \omega_1 \\ \omega_2 \\ -M^{-1}\begin{bmatrix} -p\omega_2 & -p(\omega_1+\omega_2) \\ p\omega_1 & 0 \end{bmatrix}\begin{bmatrix}\omega_1 \\ \omega_2\end{bmatrix} \end{bmatrix}_{4\times 1}
$$

then, the robot system given by (34) is simplified as

$$
\begin{cases} \dot{x} = f(x) + g(x)u \\ y = [y_1 \quad y_2]^T \end{cases}
\tag{37}
$$

which is the canonical form given by (9).

The desired trajectories are defined as $y_{d1} = \sin(t)$ and $y_{d2} = \sin(t)$, respectively. Then, the tracking errors is expressed as the form of $e = [e_1 \quad e_2]^T = [y_{d1} - y_1 \quad y_{d2} - y_2]^T$. The relative degree can be easily calculated as $r_1 = 2$ and $r_2 = 2$

$$
\begin{bmatrix} \dot{e}_1 \\ \dot{e}_2 \end{bmatrix} = \begin{bmatrix} \dot{y}_{d1} \\ \dot{y}_{d2} \end{bmatrix} - \begin{bmatrix} \omega_1 \\ \omega_2 \end{bmatrix}
$$

$$
\begin{aligned}
e^{[r]} = \begin{bmatrix} e_1^{(r_1)} \\ e_2^{(r_2)} \end{bmatrix} &= \begin{bmatrix} \ddot{y}_{d1} \\ \ddot{y}_{d2} \end{bmatrix}\\
&+ M^{-1}\begin{bmatrix} -p\omega_2 & -p(\omega_1+\omega_2) \\ p\omega_1 & 0 \end{bmatrix}\begin{bmatrix}\omega_1 \\ \omega_2\end{bmatrix} - M^{-1}\begin{bmatrix} u_1 \\ u_2 \end{bmatrix}
\end{aligned}
$$

Then, we obtain

$$
e^{[r]} = F^*(x) + G^*(x)u = v + d(x)
\tag{38}
$$

where $v = [v_1 \quad v_2]^T$ are the auxiliary inputs.

Since the relative degree of system (34) meets the condition of $r = \sum_{i=1}^{2} r_i = n = 4$, then the tacking error dynamics of (38) can be decoupled into two subsystems with inertial uncertainties as

$$
\dot{\varsigma} = \begin{bmatrix} 0 & 1 \\ 0 & 0 \end{bmatrix}\varsigma + \begin{bmatrix} 0 \\ 1 \end{bmatrix}v_1 + \begin{bmatrix} 0 \\ 1 \end{bmatrix}d_1(x)
\tag{39}
$$

$$
\dot{\tau} = \begin{bmatrix} 0 & 1 \\ 0 & 0 \end{bmatrix}\tau + \begin{bmatrix} 0 \\ 1 \end{bmatrix}v_2 + \begin{bmatrix} 0 \\ 1 \end{bmatrix}d_2(x)
\tag{40}
$$

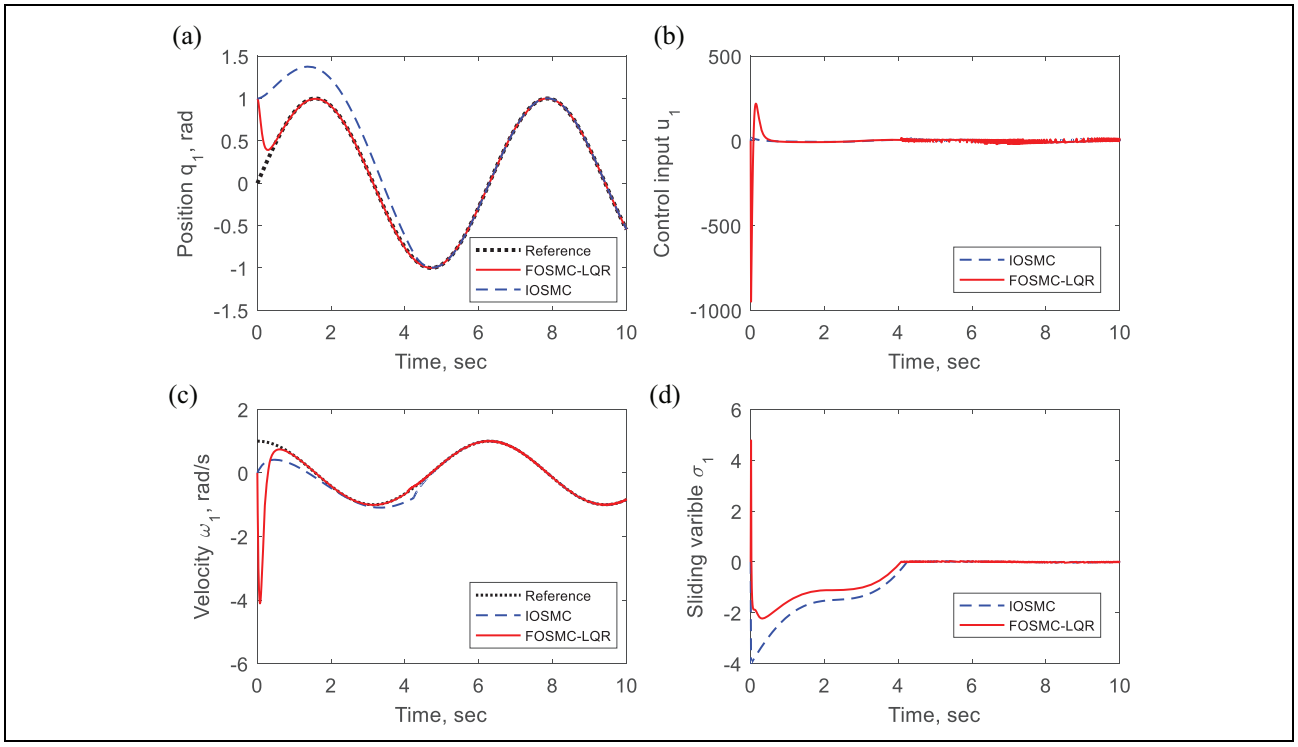

Figure 11. Tracking curves of link 1 with nominal parameters.

where $\varsigma = [e_1 \quad \dot{e}_1]^T$, $\tau = [e_2 \quad \dot{e}_2]^T$, $v_1 = v_{n1} + v_{s1}$, and $v_2 = v_{n2} + v_{s2}$. $v_{ni}(i = 1, 2)$ and $v_{si}(i = 1, 2)$ are the continuous control parts and the discontinuous control parts, respectively. $d_1(x)$ and $d_2(x)$ are the system uncertainties.

Then, the auxiliary input v can be designed according to the control design procedures in section 4.

First, let

$$Q_1 = Q_2 = Q = \begin{bmatrix} 20 & 0 \\ 0 & 0.1 \end{bmatrix}, \quad \alpha_1 = \alpha_2 = \alpha = 0.001$$

the continuous control parts $v_{n1} = -\alpha_1^{-1} B_1^T P_1 \varsigma$ and $v_{n2} = -\alpha_2^{-1} B_2^T P_2 \tau$ are derived by solving the Riccati equation (18). Then, the positive definite matrices P_1 and P_2 are calculated as

$$P_1 = P_2 = P = \begin{bmatrix} 2.7671 & 0.1414 \\ 0.1414 & 0.0196 \end{bmatrix}$$

Second, define the fractional-order sliding surfaces as $\sigma_i = \left(\frac{d}{dt} + \lambda_{i1}\right) e_i - \lambda_{i2} D^{\eta_i} e_i + v_{\text{aux}}, \dot{v}_{\text{aux}} = -v_{ni}, i = 1, 2$, the fractional control parts are obtained as

$$v_{si} = -\lambda_{i1} \dot{e}_i + \lambda_{i2} D^{\eta_i + 1} e_i - k_i \operatorname{sgn}(\sigma_i), i = 1, 2$$

By substituting v into (39), the nonlinear control law (FOSMC-LQR) is obtained as

$$u = [G^*(x)]^{-1}[v - F^*(x)] = [G^*(x)]^{-1} \left\{ \begin{bmatrix} -\alpha_1^{-1} B_1^T P_1 \varsigma - \lambda_{11} \dot{e}_1 + \lambda_{12} D^{\eta_1 + 1} e_1 - k_1 \operatorname{sgn}(\sigma_1) \\ -\alpha_2^{-1} B_2^T P_2 \tau - \lambda_{21} \dot{e}_2 + \lambda_{22} D^{\eta_2 + 1} e_2 - k_2 \operatorname{sgn}(\sigma_2) \end{bmatrix} - F^*(x) \right\}$$

In simulations, the robot initial condition is $x(0) = [1.0 \quad 1.0 \quad 0 \quad 0]^T$. The design parameters used in this simulation are chosen as follows: $\lambda_{11} = 5$, $\lambda_{12} = 1$, $\lambda_{21} = 5$, $\lambda_{22} = 1$, $k_1 = 1.5$, $k_2 = 1.5$, $\eta_1 = 0.5$, and $\eta_2 = 0.5$. Under the same conditions of switching feedback control gains k_1 and k_2, conventional IOSMCs are also designed for comparison as shown in Figures 11 to 14.

Figures 11 and 12 show a comparison of system response between the IOSMC and the controller proposed in this article (FOSMC-LQR) with nominal parameters. It can be easily seen that the closed-loop system response with FOSMC-LQR presents faster convergences of position tracking and velocity tracking. Because of choosing the same values of switching feedback control gain, the control signal presents the similar chattering when the closed-loop system is stable. However, the sliding motion of FOSMC-LQR has the faster convergence velocity in both q_1 and q_2 position channels.

Figures 13 and 14 show a comparison of system response between the IOSMC and the FOSMC-LQR with

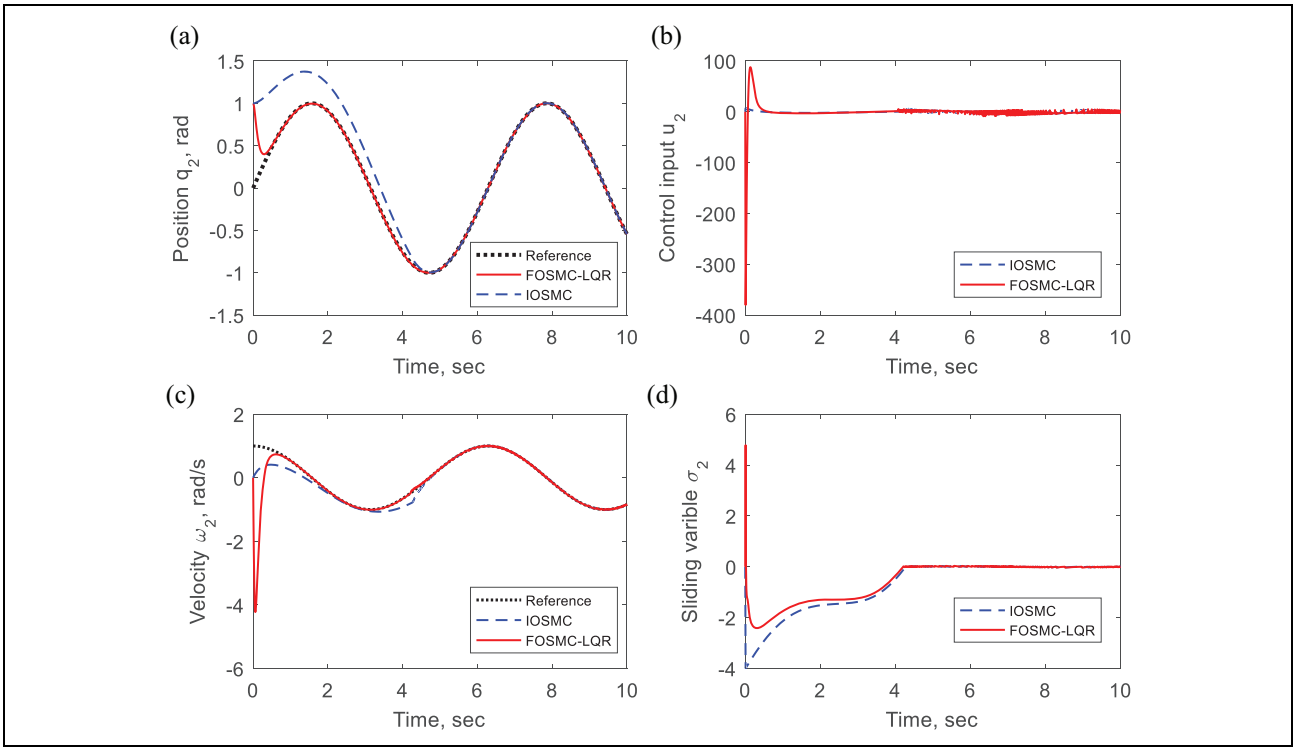

Figure 12. Tracking curves of link 2 with nominal parameters.

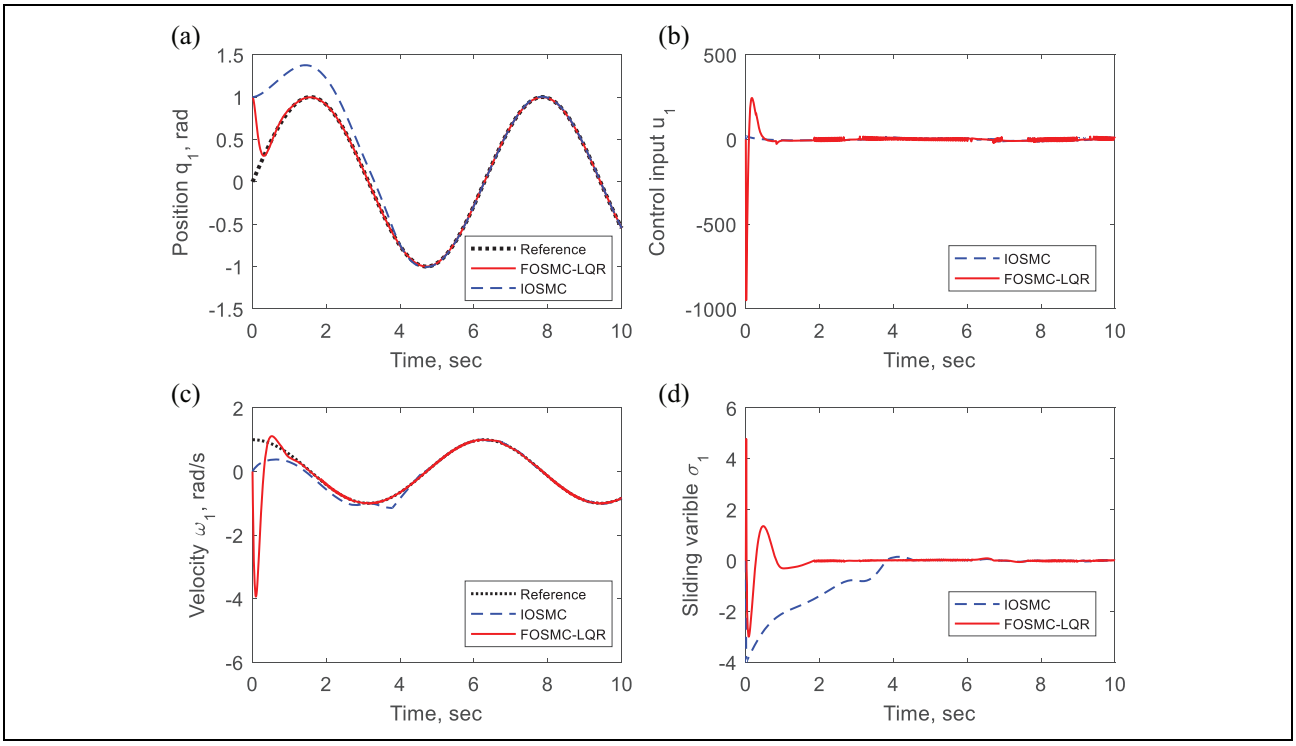

Figure 13. Tracking curves of link 1 with uncertain parameters.

uncertain parameters. And the parameter uncertainties are described by (36). Due to the existence of parameter uncertainties, the closed-loop system response with IOSMC becomes more unsteady, which presents unsteady tracking performance in position and velocity tracking channels. However, the closed-loop system with FOSMC-LQR

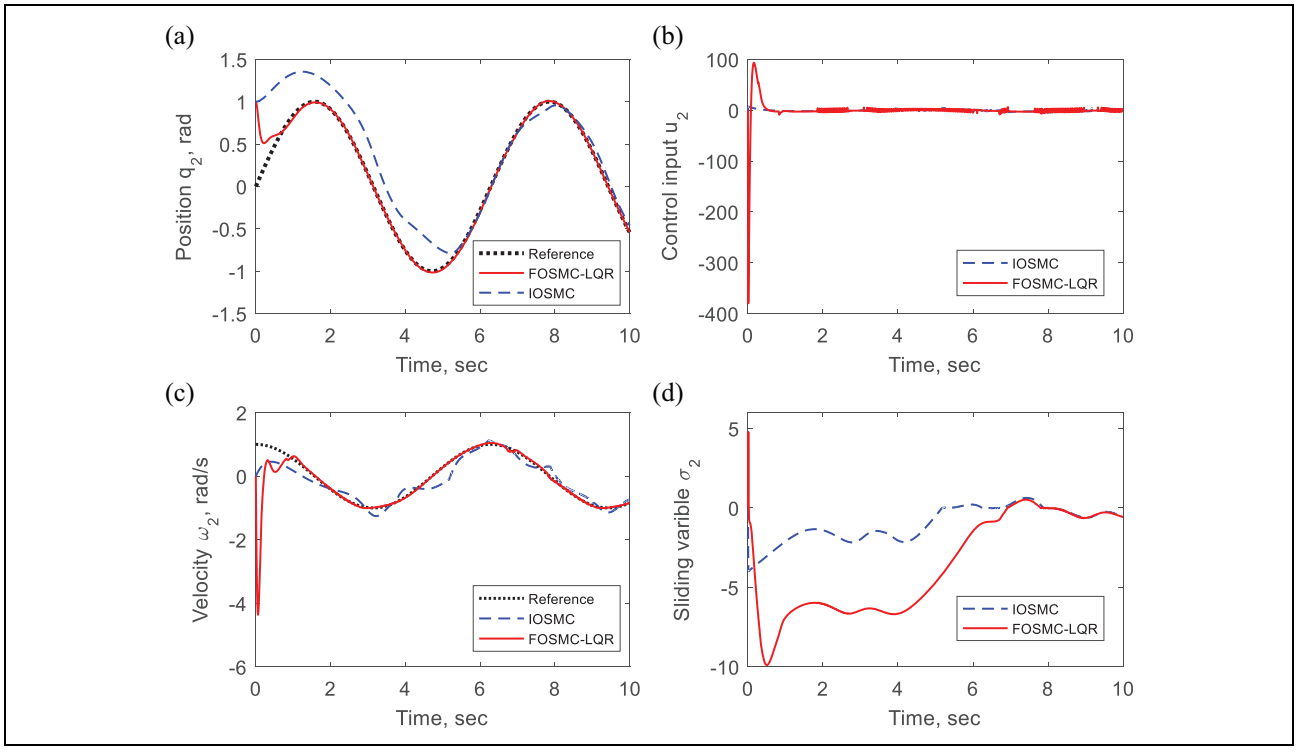

Figure 14. Tracking curves of link 2 with uncertain parameters.

successfully rejects the time-varying parameter uncertainties and presents excellent tracking robustness.

Conclusion

In this article, a new FOSMC strategy based on LQR (FOSMC-LQR) for uncertain nonlinear systems has been proposed. Lyapunov stability theory is used to prove that the proposed controller results in the finite time convergence of the sliding motion and the global stability of the closed-loop control system. To demonstrate the effectiveness and advantages of the proposed controller, two academic examples, a kinematic model of a car and a dynamic model of a two-link robot, are simulated. The results of the simulation demonstrate that the proposed controller resulted in a faster convergence velocity, better tracking performance, and excellent system robustness. The proposed controller also performed better than conventional IOSMC, single LQR, and single FOSMC because it was designed based on LQR and employed extra fractional-order derivatives of the tracking error. Moreover, the magnitude of control chattering was reduced drastically.

Acknowledgment

The authors would like to thank the National Natural Science Fund of China(Fund NO. 11672235) for their financial support and also their help with information in this work.

Declaration of conflicting interests

The author(s) declared no potential conflicts of interest with respect to the research, authorship, and/or publication of this article.

Funding

The author(s) disclosed receipt of the following financial support for the research, authorship, and/or publication of this article: This work was partly supported by the National Natural Science Fund of China (no. 11672235).

References

1. Podlubny I. *Fractional differential equations*. New York: Academic Press, 1999.
2. Uchaikin VV. *Fractional derivatives for physicists and engineers volume ii applications*. Beijing: Higher Education Press, 2013.
3. Oustaloup A. From fractality to non integer derivation: A fundamental idea for a new process control strategy. *Anaylsis and Optimization of Systems*, Paris, 2006; 53–64.
4. Oustaloup A, Sabatier J, and Lanusse P. From fractal robustness to CRONE control. *Fract Calc Appl Anal* 1999; 2: 1–30.
5. Podlubny I, Dorcak L, and Kostial I. On fractional derivatives, fractional-order dynamic systems and $PI^{\lambda}D^{\mu}$ controllers. *Conference on Decision & Control*, San Diego, December 1997, pp. 4985–4990.
6. Podlubny I. Fractional-order systems and $PI^{\lambda}D^{\mu}$ controllers. *IEEE Trans Autom Control* 1999; 44: 2108–2114.
7. Lurie BJ. Three –parameter tunable tilt-integral derivative (TID) controller, US Patent US5371 670, 1994.
8. Monje CA, Calderon AJ and Vinagre BM. The fractional order lead compensator. In: *IEEE International Conference on Computational Cybernetics*, Vienna, Austria, August 2004, pp. 347–352.

9. Tavazoei MS and Tavakoli-Kakhki M. Compensation by fractional-order phase-lead/lag compensators. *IET Control Theory Appl* 2014; 8(5): 319–329.
10. Frederico SF and Torres FM. Fractional conservation laws in optimal control theory. *Nonlinear Dynam* 2008; 53: 215–222.
11. Agrawal C and Chen YQ. An approximate method for numerically solving fractional-order optimal control problems of general form. *Comput Math Appl* 2010; 59: 1644–1655.
12. Ladcai S and Charef A. On fractional adaptive control. *Nonlinear Dynam* 2006; 43: 365–378.
13. Camacho NA and Duarte-Mermoud MA. Fractional adaptive control for automatic voltage regulator. *ISA Trans* 2013; 52: 807–815.
14. Perruquetti W and Barbot JP. *Sliding mode control in engineering*. New York: Marcel Dekker, 2002.
15. Dadras S and Momeni HR. Fractional terminal sliding mode control design for a class of dynamical systems with uncertainty. *Commun Nonlinear Sci Numer Simul* 2012; 17: 367–377.
16. Mujumdar A, Kurode S, and Tamhane B. Fractional-order sliding mode control for single link flexible manipulator. In: *2013 IEEE International Conference on Control Applications*. Hyderabad, India, 28–30 August, 2013.
17. Tang YG, Zhang XY, Zhang DL, et al. Fractional-order sliding mode controller design for antilock braking systems. *Neurocomputing* 2013; 111: 122–130.
18. Tang YG, Wang Y, Han MY, et al. Adaptive fuzzy fractional-order sliding mode controller design for antilock braking systems. *J Dynam Sys Meas Control* 2016; 138(041008): 1–8.
19. Huang JC, Li HS, Teng FL, et al. Fractional-order sliding mode controller for the speed control of a permanent magnet synchronous motor. In: *24th Chinese control and decision conference*, Taiyuan, China, May 2012, pp. 1203–1208.
20. Zhang BT, Pi YG, and Luo Y. Fractional-order sliding mode control based on parameter auto-tuning for velocity control of permanent magnet synchronous motor. *ISA Trans* 2012; 51: 649–656.
21. Aghababa MP. A fractional-order controller for vibration suppression of uncertain structures. *ISA Trans* 2013; 52: 881–887.
22. Li KN, Gao JY, and Yu F. Study on the nonsingular problem of fractional-order terminal sliding mode control. *Math Probl Eng* 2013; 523251: 1–7.
23. Yin C, Chen YQ, and Zhong SM. Fractional-order sliding mode based extremum seeking control of a class of nonlinear systems. *Automatica* 2014; 50: 3137–3181.
24. Shao SY, Chen M, and Yan XH. Adaptive sliding mode synchronization for a class of fractional-order chaotic systems with disturbance. *Nonlinear Dynam* 2016; 83(4): 1855–1866.
25. Shao SY, Chen M, Chen SD, et al. Adaptive neural control for an uncertain fractional-order rotational mechanical system using disturbance observer. *IET Control Theory App* 2016; 10(16): 1972–1980.
26. Petráš I. *Fractional-order nonlinear systems: modeling, analysis and simulation*. Berlin: Springer, 2011.
27. Monje CA, Chen YQ, Vinagre BM, et al. *Fractional-order systems and controls*. Berlin: Springer , 2010.
28. Filippov AF. *Differential equations with discontinuous right-hand side, Dordrecht*. The Netherland: Kluwer, 1988.
29. Fernández BR and Hedrick JK. Control of multivariable nonlinear systems by the sliding mode method. *Int J Control* 1987; 46(3): 1019–1040.
30. Utkin V. *Sliding modes in control optimization*. Berlin: Springer-Verlag, 1992.
31. Shtessel Y, Edwards C, Spurgeon S, et al. Adaptive finite reaching time control and continuous second order sliding modes. In: *IEEE Conference on Decision & Control*, Georgia, USA, December 2010, pp. 266–271.
32. Levant A. Higher-order sliding modes, differentiation and output-feedback control. *Int J Control* 2003; 76(9–10): 924–941.
33. Laghrouche S, Plestan F, and Glumineau A. Higher order sliding mode control based on integral sliding mode. *Automatic* 2007; 43: 513–537.
34. Dinuzzo F and Ferrara A. Higher-order sliding mode controllers with optimal reaching. *IEEE Trans automat control* 2009; 54(9): 2126–2136.
35. Slotine JJ and Li WP. *Applied nonlinear control*. New Jersey: Prentice Hall, 1991.
36. Labiod S, Boucherit MS, and Guerra TM. Adaptive fuzzy control of a class of MIMO nonlinear systems. *Fuzzy Sets Sys* 2005; 151: 59–77.